

Weakening of the slab–mantle wedge interface induced by metasomatic growth of talc

Ken-ichi Hirauchi, Sabine A.M. den Hartog, and Christopher J. Spiers

Experimental and Analytical Procedures

Starting Materials

The synthetic fault gouges used in this study were prepared from antigorite, quartz, and talc. The antigorite was collected from massive serpentinite outcropping in the Nagasaki metamorphic rocks, southwest Japan. Veins and surface coatings were removed from the samples prior to grinding. This material contains >95% antigorite, with magnetite and Cr-spinel as accessory minerals. The quartz was a pure cristobalite (a high-temperature polymorph) powder produced by the thermal treatment of α -quartz, acquired from SIBELCO. The talc was acquired from Ward's Natural Science and was collected from talc-rich schist in Balmat, New York. The antigorite and talc were crushed and sieved to <106 μm grain size, while the quartz was sieved to <50 μm . We used starting gouge materials with different compositions, including binary mixtures of 70wt% antigorite/30wt% quartz, and pure antigorite, pure talc, and pure quartz.

Deformation Experiments

In each experiment, ~0.4 g of powders was loaded onto the bottom internal piston, with the two confining rings in place (Fig. DR1). The top piston was lowered into the confining rings and fixed with the retaining screw, producing a ~1.1-mm-thick layer of simulated fault gouge. The piston-sample assembly was attached to the pressure-compensated piston plus the upper sealing head, was then lowered into the water-filled vessel, which in turn was sealed and placed into the Instron 1362 loading frame. The vessel was then moved upwards using the Instron ram, and the pressure-compensated piston was engaged with the upper forcing block plus the torque and axial force gauges.

An effective normal stress of 200 MPa was first applied using the Instron ram, then the furnace was switched on, heating to the desired temperature and applying a fluid pressure of 200 MPa. The system was subsequently left to equilibrate for 3–4 h. During this time, the sample compacted from about 40% to 10–20% porosity, i.e., to a thickness of 0.7–0.8 mm. After equilibration of the entire experimental set-up, the rotary drive was switched on to give a constant sliding velocity until a displacement of typically ~50 mm was reached.

Each experiment was terminated by removing the torque and axial load, then switching off the furnace. The system cooled to room temperature within 20 min, after which the fluid pressure was removed by venting. The piston-sample assembly was then extracted and dried in an oven at 50 °C for at least 24 h. Thin sections were prepared from the samples for petrographic analysis with an optical microscope and a scanning electron microscope (SEM). The samples were impregnated with epoxy resin before being sliced parallel to the shear direction and normal to the gouge–piston boundary. All experiments and corresponding conditions are listed in Table DR1.

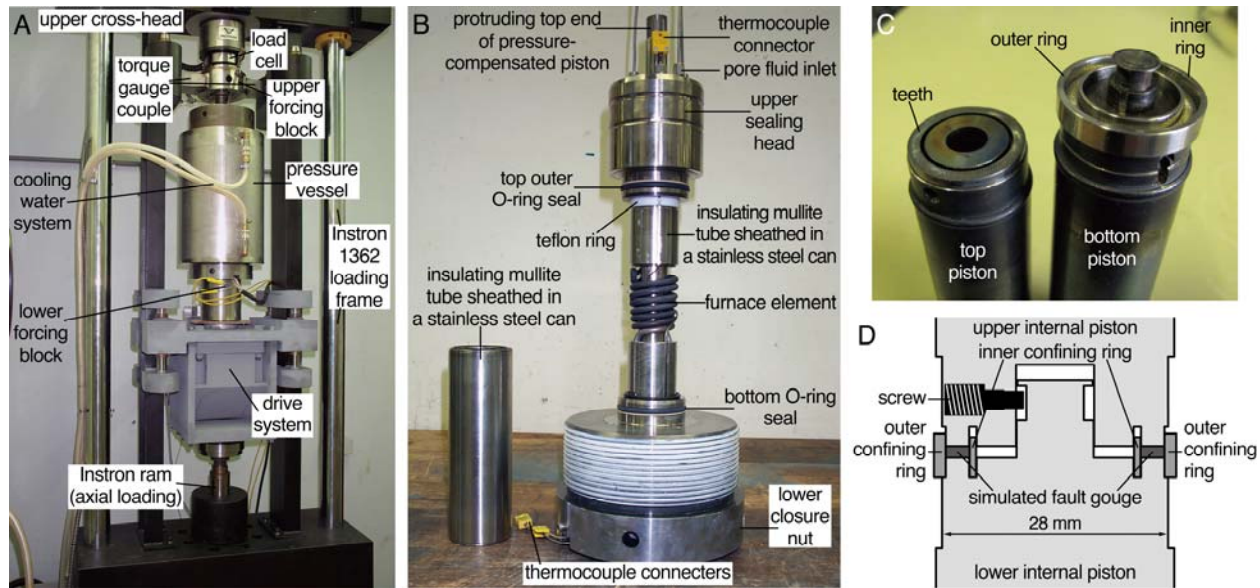


Figure DR1. Hydrothermal ring shear machine used in this study. (A) The ring shear drive system and pressure vessel located inside the Instron loading frame. (B) The two internal pistons assembled with the pressure-compensated piston plus upper sealing head. The two insulating mullite tubes, sheathed with stainless steel, and the furnace element are normally located inside the pressure vessel. (C) The two internal pistons plus sample-confining rings. (D) Schematic cross section of the piston–sample assembly.

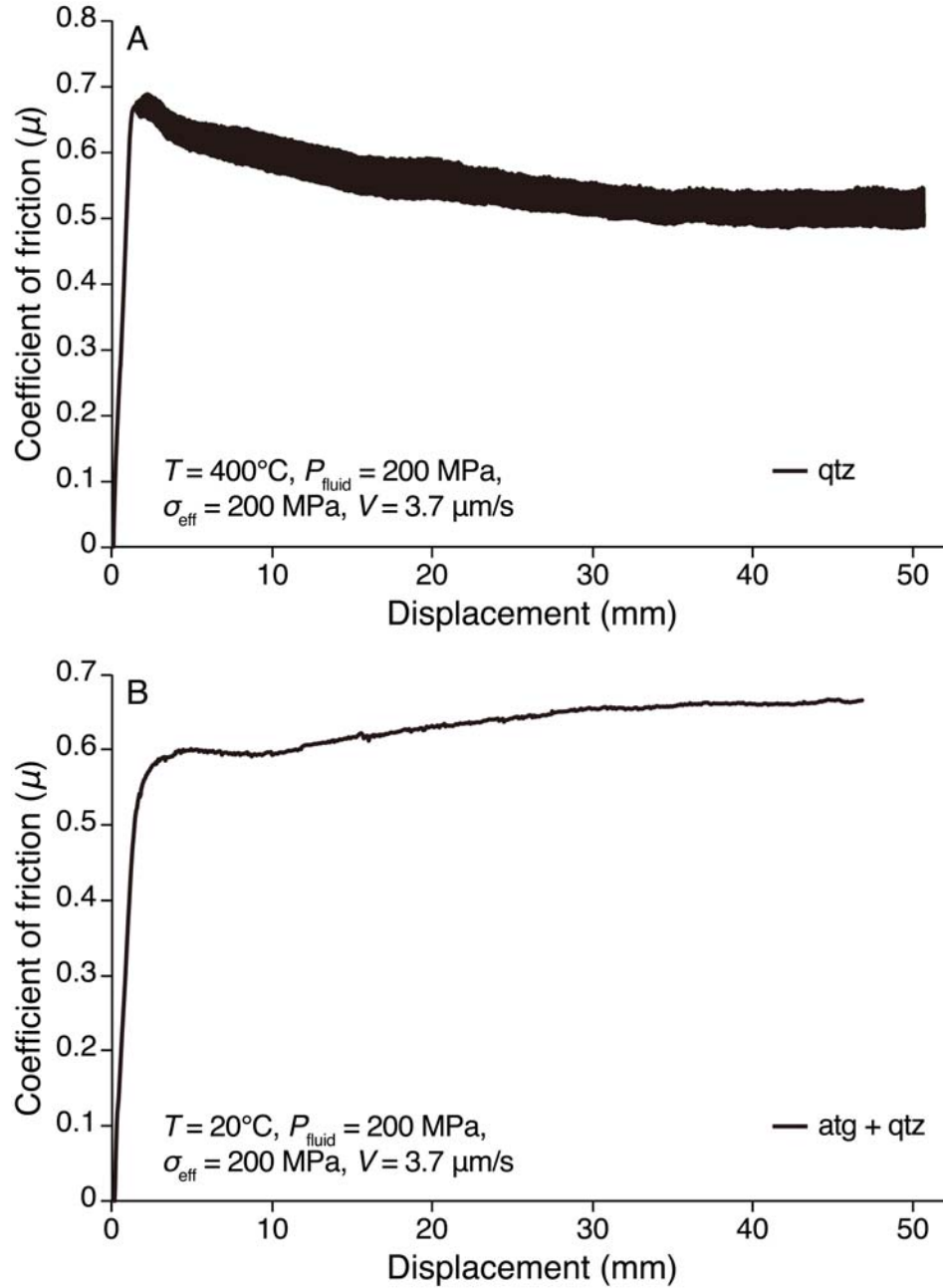


Figure DR2. Coefficient of friction as a function of shear displacement for (A) quartz and (B) antigorite–quartz mixtures. All experiments were run at a pore fluid pressure (P_{fluid}) of 200 MPa, an effective normal stress (σ_{eff}) of 200 MPa and a sliding velocity (V) of $3.7 \mu\text{m/s}$. atg: antigorite, qtz: quartz. The quartz gouge run at a temperature of 400°C showed an initial peak friction coefficient of 0.67 at $\sim 1.5 \text{ mm}$ displacement, followed by strain weakening of up to 20% towards a steady state value at $\sim 40 \text{ mm}$ displacement, with prominent stick-slip events. The antigorite/quartz gouge run at room temperature (20°C) showed an initial peak friction coefficient of 0.60 at $\sim 4 \text{ mm}$, after which strain hardening was observed until a quasi-steady state friction coefficient of 0.66 was reached at $\sim 40 \text{ mm}$ displacement.

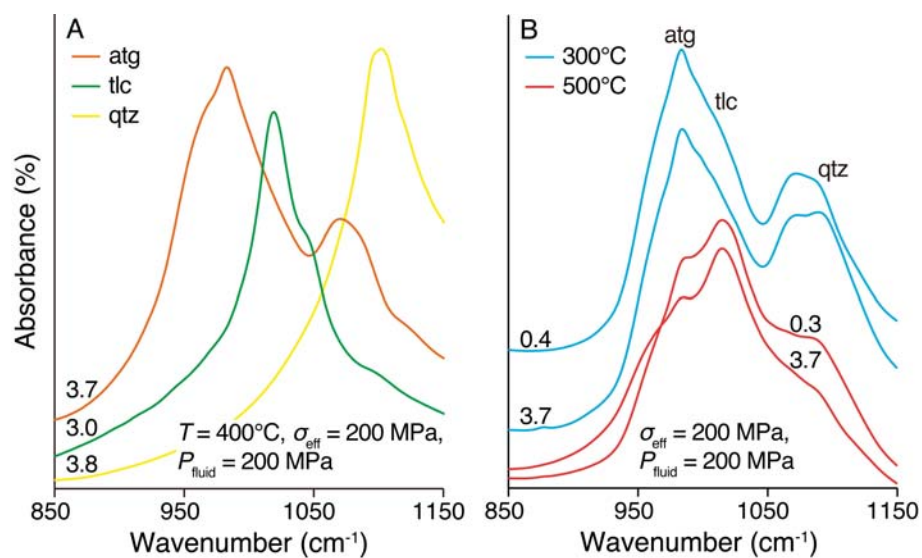


Figure DR3. FTIR spectra in the 850–1150 cm⁻¹ region for samples tested in the ring shear machine. (A) Antigorite, talc, and quartz samples at a temperature of 400 °C. (B) Antigorite–quartz mixtures at temperatures of 300 and 500 °C. Numbers adjacent to curves correspond to the sliding velocity ($\mu\text{m/s}$). atg: antigorite, tlc: talc, qtz: quartz.

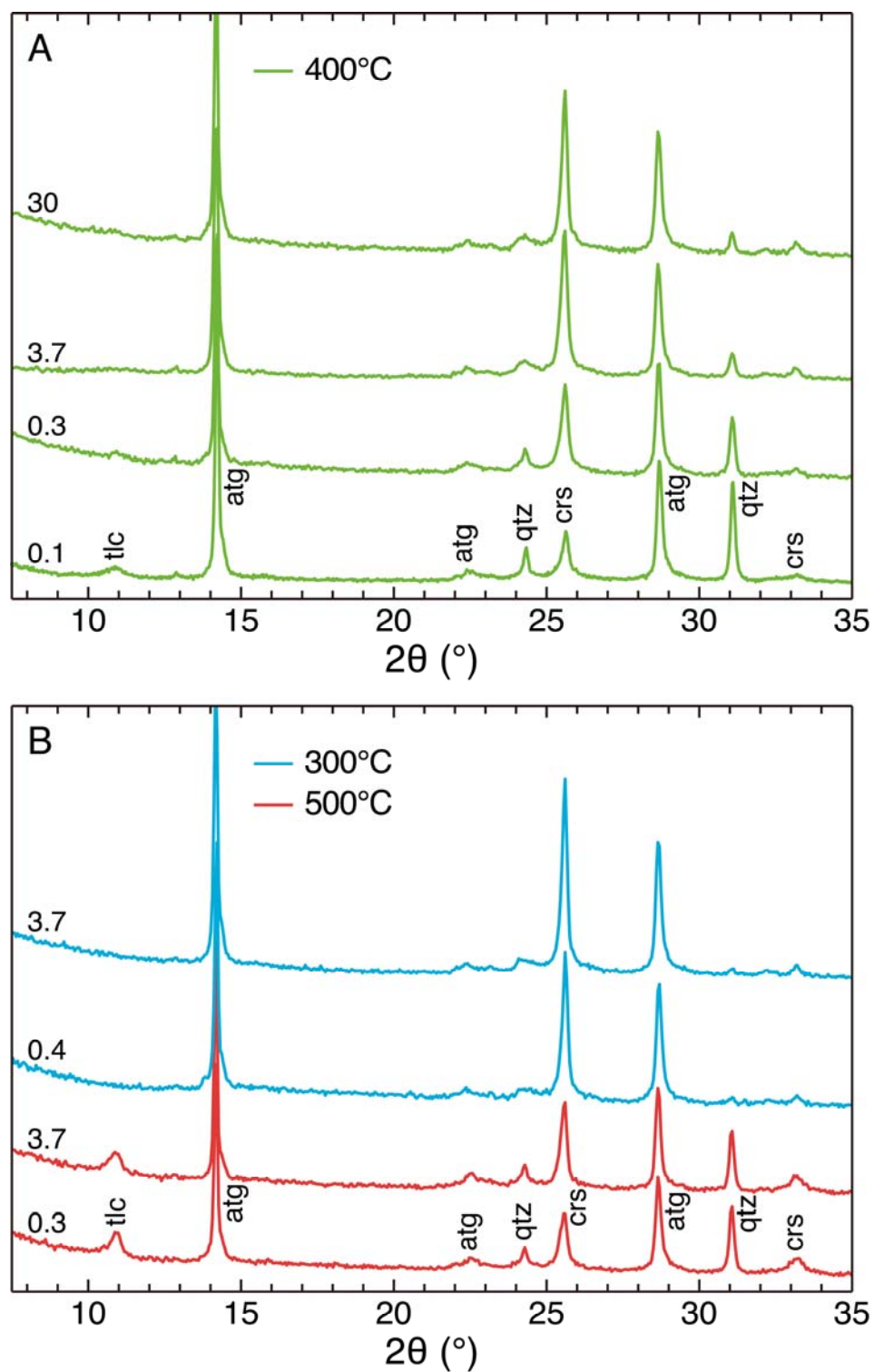


Figure DR4. X-ray diffraction (XRD) spectra for antigorite-quartz mixtures tested in the ring shear machine at three different temperatures. The XRD spectra were obtained using $\text{CoK}\alpha$ radiation with a wavelength of 1.79026\AA . Note that silica produced by dissolution of cristobalite precipitated as α -quartz, and that higher intensities of α -quartz peaks reflect larger amounts of

dissolved silica during each experiment. Numbers adjacent to curves correspond to the sliding velocity ($\mu\text{m/s}$). atg: antigorite, crs: cristobalite, tlc: talc, qtz: α -quartz. (A) $T = 400\text{ }^{\circ}\text{C}$. (B) $T = 300$ and $500\text{ }^{\circ}\text{C}$.

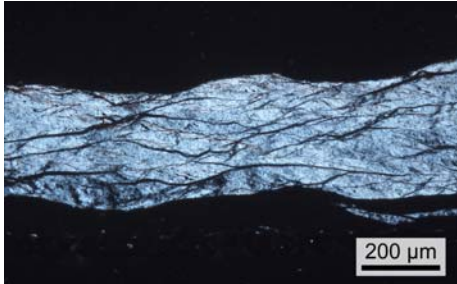


Figure DR5. Optical micrograph of pure antigorite sample (run KH-01) observed in cross-polarized light. Note the alignment of antigorite grains showing a S–C fabric, with a strong crystallographic preferred orientation.

Table DR1. Summary of all tests performed in this study

Run no.	Sample	Temperature (°C)	Pore fluid pressure (MPa)	Effective normal stress (MPa)	Sliding velocity (μm/s)	Compaction (mm)	Total displacement (mm)	Shear strain (γ)	Time (hours)
KH-01	100% atg	400	200	200	3.5	0.21	46.7	66.7	3.7
KH-02	70% atg, 30% qtz	400	200	200	3.7	0.18	50.0	71.4	3.8
KH-03	70% atg, 30% qtz	400	200	200	0.34	0.24	56.9	81.2	46.6
KH-04	70% atg, 30% qtz	400	200	200	29.6	0.22	50.3	71.9	0.47
KH-05	100% qtz	400	200	200	3.7	0.18	50.7	72.4	3.8
KH-06	70% atg, 30% qtz	300	200	200	3.7	0.23	51.1	73.0	3.8
KH-08	70% atg, 30% qtz	500	200	200	0.35	0.16	46.1	65.8	36.6
KH-09	70% atg, 30% qtz	500	200	200	3.7	0.21	49.6	70.8	3.7
KH-10	70% atg, 30% qtz	300	200	200	0.35	0.25	52.8	75.4	41.9
KH-11	70% atg, 30% qtz	400	200	200	0.097	0.29	48.5	69.4	139.3
KH-12	100% tlc	400	200	200	3.9	0.33	41.3	59.0	3.0
KH-13	70% atg, 30% qtz	400	200	200	0.37	0.09	2.8	4.1	2.1
KH-16	70% atg, 30% qtz	400	200	200	0.38	0.19	20.6	29.4	15.2
KH-19	70% atg, 30% qtz	20	200	200	3.67	0.20	46.9	67.0	3.6

atg–antigorite, qtz–quartz, tlc–talc.